AIAA JOURNAL
Vol. 35, No. 10, October 1997

Surface Reflective Visualizations of Shock-Wave/Vortex Interactions Above a Delta Wing

S. R. Donohoe* and W. J. Bannink†
Delft University of Technology, 2629 HS Delft, The Netherlands

The surface reflective visualization (SRV) system is used to investigate the vortical flowfield above a 65-deg sweep, sharp leading-edge, noncambered delta wing in a high subsonic flow. Configurations of M_∞–α are considered that both do and do not exhibit vortex breakdown above the wing, with and without the presence of a terminating shock-wave system above the wing. The SRV system provides a new opportunity to investigate the behavior of vortex breakdown in the high subsonic regime as well as the spanwise distribution of the terminating shock-wave system above the wing. Two classes of vortex breakdown, asymmetric and symmetric, are observed. The terminating shock-wave system is found to influence vortex breakdown and wing performance in the presence of vortex breakdown.

Nomenclature

$\bar{C}_p$ = average surface pressure coefficient
c_r = root chord, 120 mm
f = focal length
I = illumination
n = refractive index
t = time
x = chordwise distance from wing apex
y_{le} = local spanwise distance from root chord to leading edge
α = angle of attack
κ = Gladstone–Dale constant

I. Introduction

TO achieve an attractive balance between supersonic cruise performance and maneuverability at high subsonic speeds, modern aircraft designers often utilize highly swept slender wings or delta wings. These aircraft achieve high maneuverability by exploiting the nonlinear lift component generated by the powerful rotating flow existing above the lee surface of the wing when operating at angle of attack (Fig. 1). At a given freestream Mach number, the nonlinear lift component generated by existing leeside vortices will increase with increasing angle of attack up to the point where the vortex breaks down. Vortex breakdown is commonly described as a transition from an organized vortical flow structure to a large-scale fluctuating turbulent flow. In the incompressible flow regime, the breakdown position above the wing is found to move gradually forward with increasing angle of attack. In the compressible regime, however, breakdown has been noted to jump suddenly from beyond the trailing edge to as far forward as 50% of the wing chord at a critical angle of attack.[1] The sudden presence of vortex breakdown above the wing, which is often asymmetric with respect to the symmetry plane of the wing, can lead to control problems for the aircraft. The vortex breakdown process is particularly complex in the high subsonic flow regime where the vortex flow is influenced by compressible flow effects such as shock-wave/vortex and shock-wave/boundary-layer interactions. In his recent survey of the last 40 years of vortex breakdown research, Délery[2] admits that despite its importance for high-speed flight "the question of shock/vortex interaction and shock-induced breakdown" remains "a largely unexplored field."

The surface reflective visualization (SRV) technique has been developed[3] and validated[4] to investigate this flow problem. The SRV system provides a plan-view perspective of the integrated-density distribution above a noncambered delta wing. This top-view perspective provides new information on vortices, shock waves, and vortex/shock-wave interactions above the delta wing. Large-scale flow fluctuations and the unsteady shock-wave system associated with vortex breakdown can be visualized by incorporating a high-speed drum camera and spark light source (exposure time $\approx$20 ns) into the SRV system configuration. The high-speed camera used in this investigation incorporates a rotating inner drum, about which 35-mm film is stretched, to capture a maximum of 70 consecutive exposures at high frequency (maximum frequency 10 kHz).

In the current investigation the SRV technique is used to examine the flowfield of a 65-deg sweep, noncambered, 120-mm root chord, sharp leading-edge delta wing in the high subsonic flow regime. The test matrix consists of three freestream Mach numbers (0.6, 0.7, and 0.8) and three angles of attack (15, 18, and 20 deg.). All tests are performed in the TST-27 transonic–supersonic blow-down wind tunnel of the Delft University of Technology High Speed Aerodynamics Laboratory (tunnel cross section $\approx$280 $\times$ 260 mm).

II. SRV System

The SRV system is a derivative of a double-pass schlieren/shadow-graph system in which the model surface is itself a mirror and a component of the optical system (Fig. 2). The main optical component of the system is a parabolic mirror, which projects a parallel bundle of light into the test section along a path perpendicular to the upper surface of the model. Because the upper surface of the model is a mirror surface, the light is reflected back along nominally the same path to the parabolic mirror and brought to focus on the image plane of the camera.

By definition, a schlieren system produces a two-dimensional image of a component of the density gradient existing perpendicular to a parallel light bundle integrated over the path of the bundle. The component of the density gradient that is visualized is determined by the orientation of the schlieren knife edge. Specifically, the change in illumination at a location (x, y) in a schlieren image relative to that of the undisturbed image is described by the relation

$$\frac{\Delta I}{I}(x, y) \propto \int_0^L \frac{\partial}{\partial y} n(x, y, z)\, \mathrm{d}z \tag{1}$$

where the refractive index n is linearly coupled to the density via the relation

$$n = 1 + \kappa\rho \tag{2}$$

The schlieren knife edge is in the x–y plane parallel to the x axis, and the z axis is aligned with the path of the parallel light bundle. The integral taken from 0 to L follows the path of the bundle of light. The Gladstone–Dale constant κ, a characteristic of the gas through which the light passes, is a weak function of the light wavelength and

Received Jan. 29, 1996; revision received Feb. 5, 1997; accepted for publication June 9, 1997.

*Research Assistant, Department of Aerospace Engineering, Kluyverweg 1. Student Member AIAA.
†Associate Professor, Aerospace Engineering, Department of Aerospace Engineering, Kluyverweg 1.

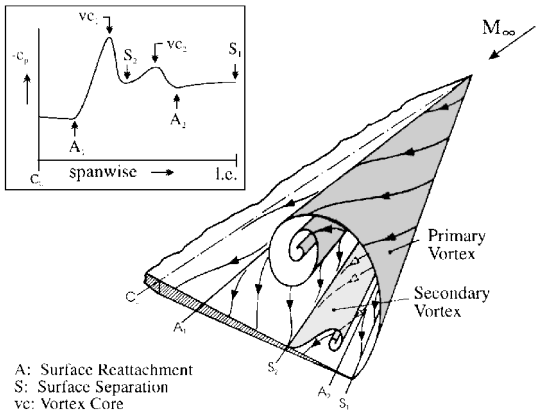

Fig. 1 Vortical flow about a sharp leading-edge delta wing at angle of attack and its associated surface pressure distribution.

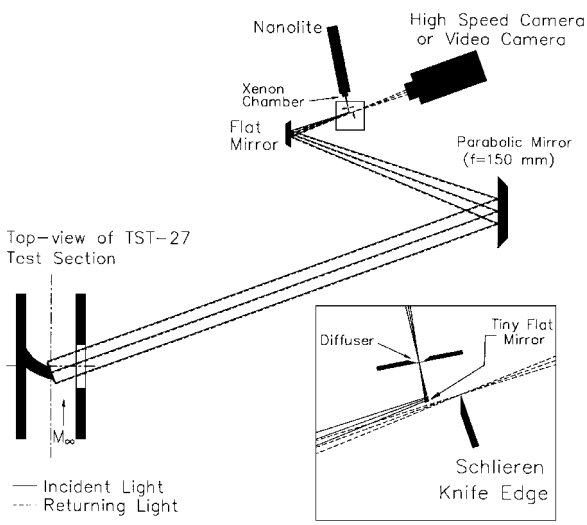

Fig. 2 SRV system configuration.

nearly independent of pressure and temperature.[5] To assist interpretation of SRV images, which provide a two-dimensional image of a three-dimensional flowfield, several images were simulated from independent experimental and numerical data in a system analysis study.[4] The subsequent discussion is supported by this system analysis study.

In the SRV system configuration used primarily in this study, the schlieren knife edge is aligned parallel with the root chord. Thus, the image produced illustrates the distribution of the spanwise density gradient integrated along a path perpendicular to the model surface. An example of an image produced with the knife edge aligned parallel to the root chord of the model is shown in Fig. 3a. The gradients in the spanwise direction of the inboard half of the primary vortices are represented by the light and dark colored bands on the port and starboard sides of the wing, respectively. Crossflow shock waves, embedded between the primary vortices and the wing surface, are visible as sharp dark and light colored lines, outboard of these bands, on the port and starboard sides, respectively (Fig. 4). The dark line, intersecting the chord at approximately 80% of the root chord, represents a terminating shock wave. Theoretically, the terminating shock-wave system, exhibiting density gradients mainly in the chordwise direction, should not be visualized by a schlieren system with the knife edge aligned with the chord. This shock wave is visualized due to the presence of a tiny mirror at the junction of the outgoing and returning light bundles. Shock waves causing a large deflection of the light, due to their strength or extent along the path of the light, will cause the light to deflect outside the path of the returning bundle and impact this tiny mirror. The tiny mirror functions, thus, as an effective schlieren knife edge oriented perpendicular to the root chord when large deflections of light occur. The projection of the primary vortex core location onto the wing surface, defined as the location of minimum total pressure obtained via five-hole probe measurements,[4] is also indicated in Fig. 3a for reference purposes.

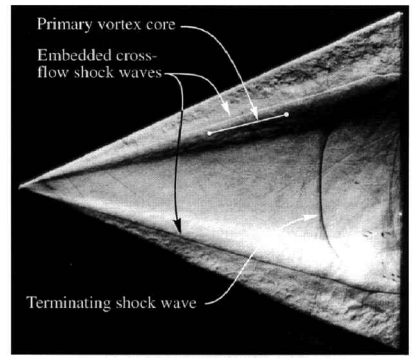

a) Knife edge parallel with root chord

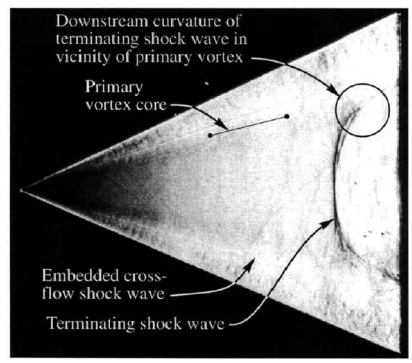

b) Knife edge perpendicular to root chord

Fig. 3 SRV images, top view: $M_\infty = 0.8$ and $\alpha = 15$ deg.

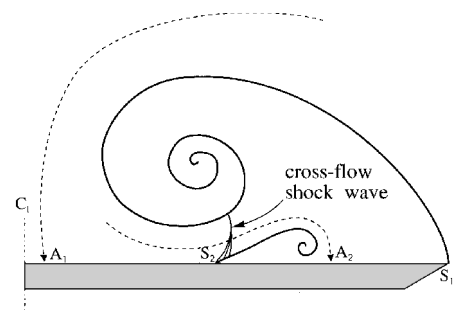

Fig. 4 Illustration of embedded crossflow shock wave.

The distribution of the chordwise density gradient, integrated along a path perpendicular to the model surface, can be produced by aligning the schlieren knife edge perpendicular to the root chord. This configuration is particularly useful in examining flow configurations exhibiting a terminating shock-wave system. An example of an SRV image produced with this system configuration is shown in Fig. 3b. A terminating shock wave is noted to intersect the root chord at $(x/c_r) \approx 0.80$. This shock wave extends outboard toward the leading edge, on either side of the wing, and curves downstream toward the trailing edge in the vicinity of the primary vortices.

III. Results

The state of the leading-edge vortex system, i.e., with or without vortex breakdown occurring above the wing, for each of the M_∞–α configurations investigated is shown in Table 1. When no vortex breakdown is present above the wing, an organized and nearly conical vortex geometry is observed over the entire length of the wing. In the case of symmetric vortex breakdown, an abrupt termination of this organized vortex structure is observed at the same location ($\pm$15% of the root chord) on either side of the root chord for the duration of one rotation of the high-speed camera ($t = 35$ ms, exposure frequency $= 2$ kHz). The flowfield is noted to be highly unsteady in the case of asymmetric vortex breakdown. The vortex breakdown location may be identical on either side of the root chord or differ by as much as 40% of the root chord in the course of one exposure

Table 1 State of leading-edge vortex system for each of the M_∞–α configurations considered

	Angle of attack, deg			
M_∞	10	15	18	20
0.6	NB[a]	NB	NB	SymB[b]
0.7	NB	NB, TS[c]	AsymB,[d] TS	SymB, TS
0.8	NB, TS	NB, TS	AsymB, TS	SymB, TS

[a] No vortex breakdown.
[b] Symmetric vortex breakdown.
[c] Terminating shock wave system observed.
[d] Asymmetric vortex breakdown.

series of the high-speed camera (again, $t = 35$ ms). At least five separate tests are performed at each M_∞–α configuration to ensure the repeatability of results. Configurations that exhibit a terminating shock-wave system are also indicated in Table 1. Vortex breakdown is noted to occur both with and without a terminating shock-wave system present above the wing.

New insights into the flowfield above a delta wing in the high subsonic flow regime obtained via application of the SRV technique are presented next. The structure of the terminating shock-wave system and the nature of vortex breakdown in this flow regime are investigated. Interpretation of the results is supported, where appropriate, by data obtained in previously performed five-hole probe measurements, surface pressure measurements, and side-view transmission schlieren visualizations.

A. Sustained Vortex System

At $\alpha = 15$ deg, no vortex breakdown is observed above the wing for any of the freestream Mach numbers considered. A terminating shock-wave system is observed in the cases of $M_\infty = 0.7$ and 0.8. The SRV images of Fig. 3 illustrate a single terminating shock wave present near the trailing edge when $M_\infty = 0.8$ and $\alpha = 15$ deg. As mentioned earlier, Fig. 3a is made with the schlieren knife edge oriented parallel with the chord and Fig. 3b with the schlieren knife edge aligned perpendicular to the root chord. A side-view transmission schlieren image of a terminating shock wave for this same M_∞–α configuration is shown in Fig. 5. It is difficult to determine which SRV image corresponds with this transmission visualization image exactly due to the logistical inability to make simultaneous exposures with both systems. Based on the known behavior of the schlieren system and knowledge of the flowfield obtained via other experimental techniques, however, it is possible to draw some conclusions regarding the geometry of the shock surface above the wing.

The line clearly visible as a shock wave in the side-view transmission image of Fig. 5 can be associated with the foremost portion of the shock surface extending perpendicularly from the root chord on either side of the wing in Figs. 3a and 3b. This conclusion can be drawn because the light refraction imaged by a schlieren system is a function of both the extent of the density gradient along its path, as well as the strength of that gradient [see Eq. (1)]. The section of the shock surface extending perpendicular to the root chord and, thus, parallel with the transmission light bundle, can be expected to be more clearly illustrated in the side-view schlieren image with the knife edge oriented perpendicular to the freestream, therefore, than other portions of the shock surface. Thus, the section of the shock surface in the vicinity of the root chord is shown in the side-view transmission image to extend from the surface of the wing, curve upward concave to the apex, and extend above the wing nearly perpendicularly with the oncoming flow until it vanishes.

The downstream curvature of the shock surface in the vicinity of the primary vortices is consistently present in all top-view visualizations of the terminating shock-wave system. The fact that the terminating shock wave does not disrupt the organized vortex structure in the vicinity of the trailing edge (see Fig. 3a) suggests that it is, in fact, situated above the primary vortex in this region for this M_∞–α configuration. The presence of embedded crossflow shock waves extending to the trailing edge, only feasible in the presence of a highly organized and powerfully rotating vortex structure, further substantiates the undisturbed state of the vortex structure in the vicinity of the trailing edge. This shock wave functions to realign the flow coming over the top of the primary vortex with the freestream flow at the trailing edge. A concept sketch of the possible shock wave structure is shown in Fig. 6. The geometry of the shock wave as it moves outboard and up onto the top of the vortex structure remains unclear.

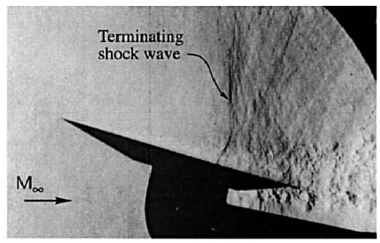

Fig. 5 Sideview transmission schlieren image with schlieren knife edge oriented perpendicular to the freestream: $M_\infty = 0.8$ and $\alpha = 15$ deg.

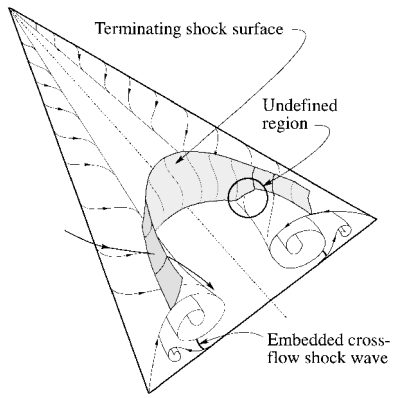

Fig. 6 Terminating shock surface in presence of sustained leading-edge vortex system.

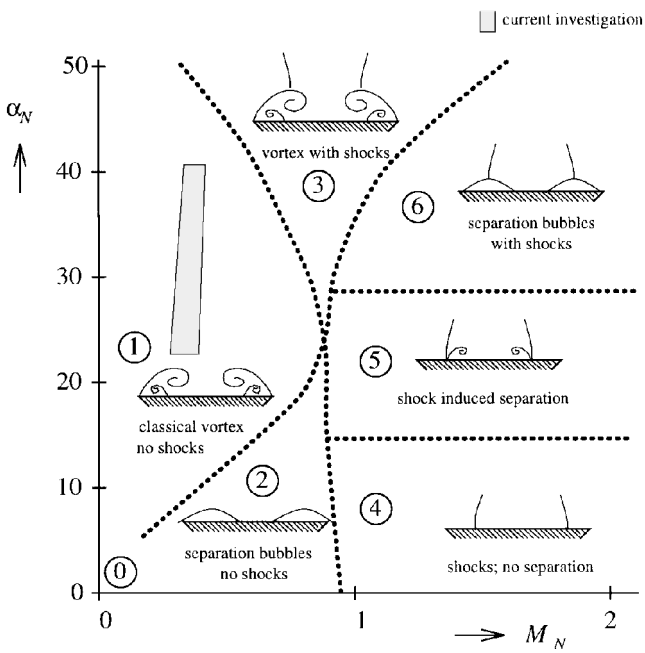

Fig. 7 Classification of leeward flow patterns over thin delta wings.[6]

Note the similarities between the proposed terminating shock wave structure and the conical shock wave structure shown in region 3 of the Miller and Wood[6] diagram developed for the case of an infinite wing (Fig. 7). Whereas the presence of a terminating shock wave is only possible in the case of a finite wing, the downstream curvature of the terminating shock wave in the vicinity of the primary vortex suggests a conical geometry of the terminating shock wave. When $M_\infty = 0.8$ and $\alpha = 15$ deg, the associated values of $M_N = 0.39$ and $\alpha_N = 32.4$ place this configuration in region 1, but in the vicinity of region 3 on the Miller and Wood[6] diagram. It seems likely that, whereas no shock waves are present above the vortices along the entire length of the wing, i.e., no conical shock waves, the pressure rise associated with the trailing edge is sufficient to provoke such shock waves above the primary vortices in the vicinity of the trailing edge.

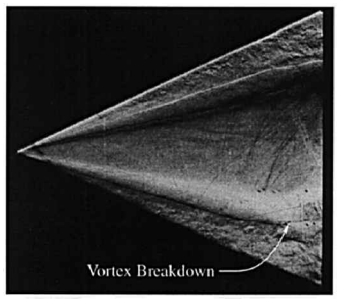

a) SRV, run 136, knife edge parallel with root chord

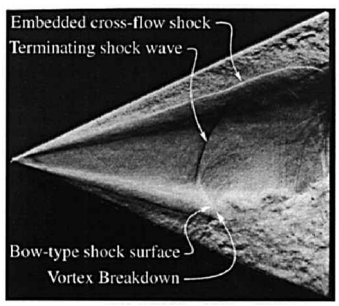

b) SRV, run 136, knife edge parallel with root chord

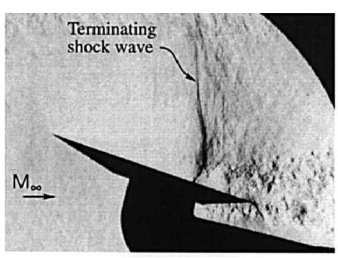

c) Transmission schlieren, knife edge perpendicular to freestream

Fig. 8 Images: $M_\infty = 0.8$ and $\alpha = 18$ deg.

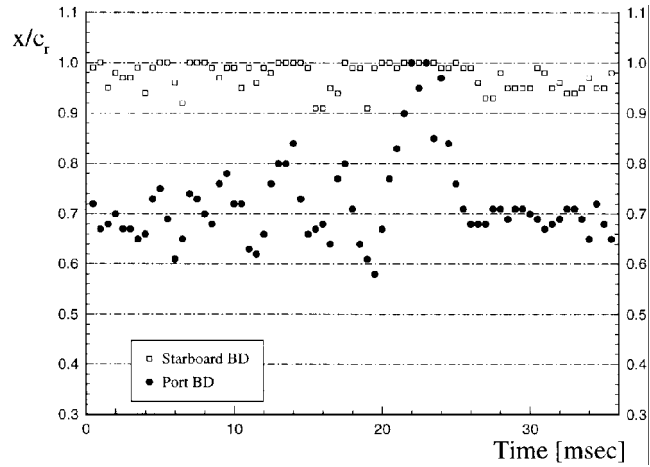

a) Run 136, predominantly port breakdown

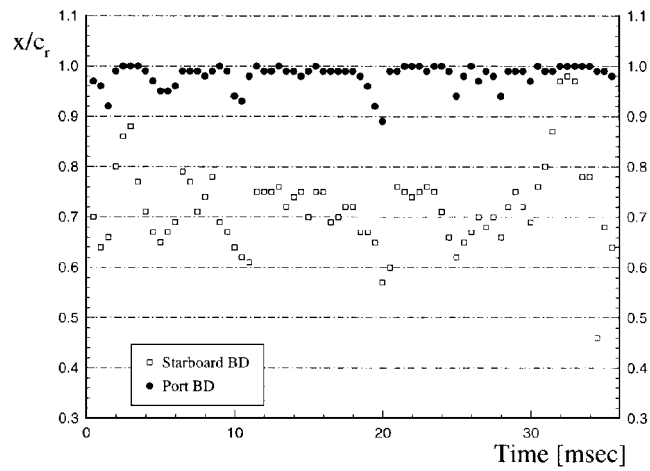

b) Run 134, predominantly starboard breakdown

Fig. 9 Vortex breakdown location on either side of the wing: $M_\infty = 0.8$ and $\alpha = 18$ deg.

B. Asymmetric Vortex Breakdown

The unsteady nature of the flowfield in the case of asymmetric vortex breakdown is shown in Figs. 8a and 8b. These two images, taken during one rotation of the high-speed camera ($\Delta t < 35$ ms), illustrate a large discrepancy in the position of vortex breakdown location on the port side of the wing. The vortex breakdown location on either side of the wing for the duration of this same test is shown in Fig. 9a. The point of vortex breakdown is defined as the chordwise position of a visible disruption of the organized primary vortex structure (Fig. 8b). The breakdown location data in this investigation are taken exclusively from SRV images configured with the schlieren knife edge aligned parallel with the root chord to ensure consistent determination of the vortex breakdown location. Images where no vortex breakdown is observed above the wing are indicated as $(x/c_r) = 1.0$. In Fig. 9a, vortex breakdown is noted to occur predominantly on the port side of the wing. In contrast, vortex breakdown is evident predominantly on the starboard side of the wing in run 134 at this same M_∞–α configuration (Figs. 9b and 10a).

The projection of the terminating edge shock wave, observed in the side-view transmission schlieren visualization image of Fig. 8c, onto the upper surface of the wing is seen in Fig. 8b. The transmission schlieren image is, as are the SRV images, produced with a spark light source of approximately 20-ns exposure time. The highly unsteady nature of the terminating edge shock-wave system is observed in both the transmission schlieren and SRV images. Although it is, again, difficult to determine which SRV image corresponds with which transmission visualization image exactly due to the logistical inability to make simultaneous exposures with both systems, some conclusions can be drawn.

The foremost and uppermost part of the shock wave in Fig. 8c corresponds geometrically with the foremost part of the projected shock wave intersecting the root chord nearly perpendicularly in Fig. 8b. The lower and more curved section of the shock wave in Fig. 8c is attributed to the section of the shock surface interacting with the vortex breakdown slightly farther downstream, while some curvature of the shock surface in the vicinity of the root chord may also be present (as mentioned in the case of no vortex breakdown discussed earlier). The bow-type shock wave in the vicinity of the primary vortex is likely an important mechanism in the vortex breakdown process. The presence of a shock wave in the vicinity of the primary vortex core will decelerate the flow along the vortex core.

Similar to the terminating shock wave in the presence of a sustained vortex system, the section of the shock surface extending downstream nearly parallel with the embedded crossflow shock on the port side of the wing in Fig. 10a is likely located above the organized vortex structure. This conclusion is, again, supported by the undisturbed state of the port-side vortex and the embedded crossflow shock wave coexisting with the terminating shock-wave surface on the port side of the wing. The formation of the terminating shock surface on the port side of the wing (Fig. 10b) is influenced by the presence of vortex breakdown on the starboard side of the wing. Whereas the exact geometry of the flow beyond the point of vortex breakdown is uncertain, a loose spiral structure is visible on the starboard side of the wing in the SRV image of Fig. 10a. This less organized structure creates an obstruction for the flow moving downstream in the vicinity of the root chord. Therefore, the terminating shock surface becomes necessary to allow the supersonic flow moving over the top of the port vortex to navigate the obstruction of vortex breakdown on the starboard side of the wing as well as the impending trailing edge pressure rise.

C. Symmetric Vortex Breakdown

Symmetric vortex breakdown is observed at $\alpha = 20$ deg for all three freestream Mach numbers investigated. The three M_∞–α

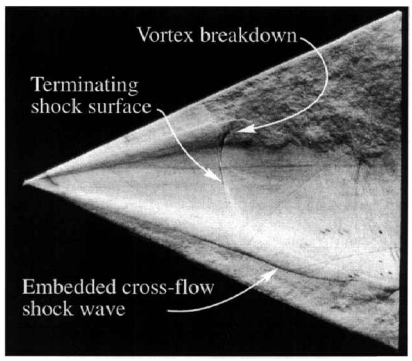

a) SRV image, run 134, knife edge parallel with root cord, $M_\infty = 0.8$, $\alpha = 18$ deg

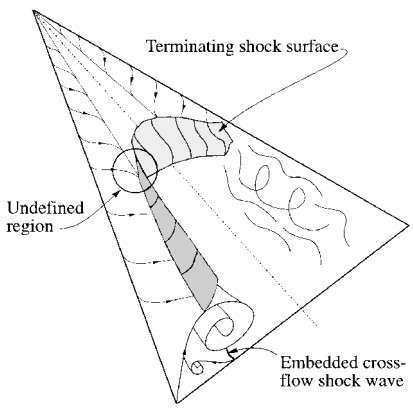

b) Concept sketch of three-dimensional shock structure

Fig. 10 Asymmetric vortex breakdown and terminating shock wave.

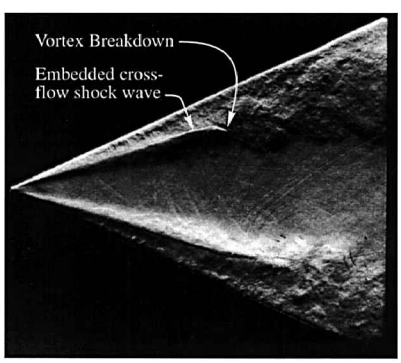

Fig. 11 SRV image, knife edge parallel with root chord: $M_\infty = 0.6$ and $\alpha = 20$ deg.

configurations where symmetric vortex breakdown is observed in this investigation, however, represent significantly different flowfields. No terminating shock-wave system is visible in the SRV images when $M_\infty = 0.6$ (Fig. 11), whereas at $M_\infty = 0.7$ and 0.8 a terminating shock-wave system is visible in the SRV images. For the case of $M_\infty = 0.8$ a double-shock terminating shock-wave system is visible in both Figs. 12a and 12b. The formation of a double-shock system results from the acceleration of the flow along the wing centerline beyond the first shock wave due to the presence of vortex breakdown on either side of the wing. The flow obstruction associated with vortex breakdown results in an effective nozzle about the wing centerline.[7]

The variation of the vortex breakdown location during the course of one high-speed photograph series ($t = 35$ ms) for two symmetric breakdown configurations is shown in Fig. 13. The vortex breakdown position on either side of the wing, while not fluctuating in phase, are more similar to each other over the course of these runs than the asymmetric vortex breakdown fluctuations shown in Fig. 9. Note that, although a strong terminating shock-wave system is present in the case of $M_\infty = 0.8$ and no terminating shock-wave

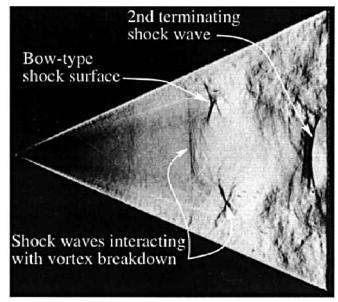

a) Knife edge perpendicular to the root chord

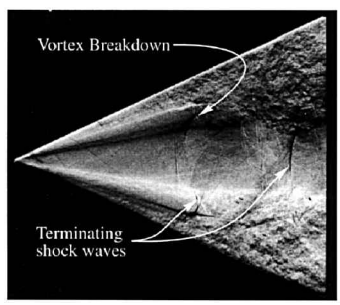

b) Knife edge parallel with the root chord

Fig. 12 SRV images: $M_\infty = 0.8$ and $\alpha = 20$ deg.

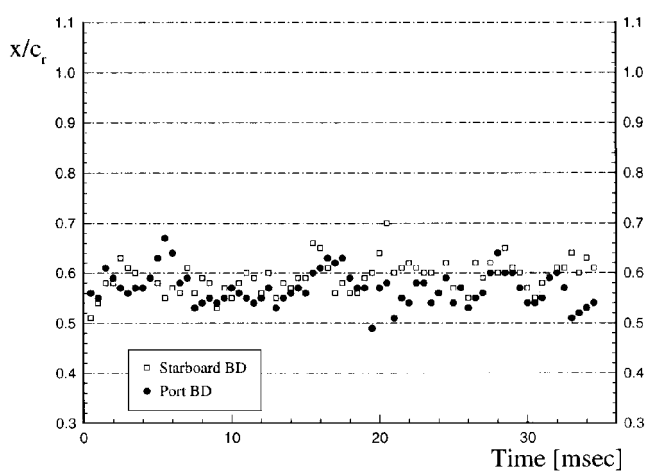

a) $M_\infty = 0.6$, run 117

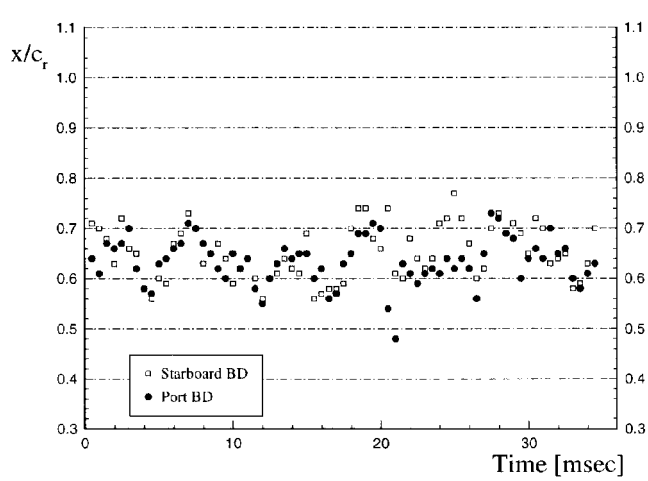

b) $M_\infty = 0.8$, run 160

Fig. 13 Vortex breakdown location on either side of the wing, $\alpha = 20$ deg.

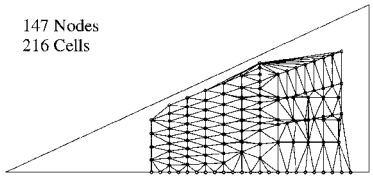

Fig. 14 Surface pressure measurement grid.

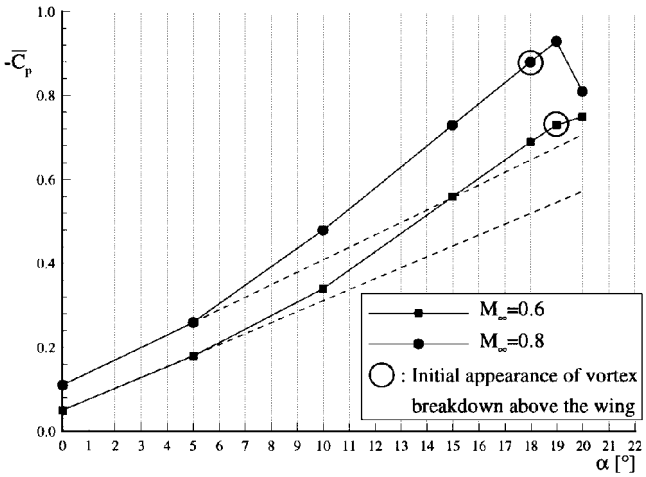

Fig. 15 Variation of average surface pressure coefficient $\bar{C}_p$ with angle of attack and freestream Mach number.

system is present in the case of $M_\infty = 0.6$, the vortex breakdown fluctuations in Figs. 13a and 13b are very similar.

To investigate the influence of vortex breakdown on wing performance, an average surface pressure coefficient $\bar{C}_p$ is defined. This quantity is defined as the sum of the average $\bar{c}_p$ value for each of the cells shown in the surface pressure measurement grid of Fig. 14 divided by the total surface area of that measurement grid. The measurement grid encloses 61% of the total wing upper surface and spans between approximately 40 and 90% of the root chord. Although this average surface pressure coefficient does not provide a true measurement of wing lift, it does provide some indication of the influence of the state of the vortical flowfield on the wing performance.

The variation of $\bar{C}_p$ with angle of attack ($0 \leq \alpha \leq 20$) is shown in Fig. 15 for $M_\infty = 0.6$ and 0.8. An estimation of the linear lift, linearly extrapolated from the two smallest α configurations at each Mach number, is indicated for reference purposes. The angle of attack at which vortex breakdown initially appears above the wing is also indicated in Fig. 15. In the case of $M_\infty = 0.6$, the value of $\bar{C}_p$ continues to increase with angle of attack beyond the initial appearance of vortex breakdown above the wing. The slope is noted to decrease, however, between 19 and 20 deg. Similarly, in the case of $M_\infty = 0.8$, the value of $\bar{C}_p$ continues to increase with angle of attack beyond the initial appearance of asymmetric vortex breakdown above the wing and to decrease only between 19 and 20 deg.

A similar trend of increasing lift with angle of attack beyond the initial appearance of vortex breakdown above the wing was observed in the force balance measurements of Erickson et al.[8] These measurements, conducted on a sharp leading-edge delta wing with the freestream Mach numbers ranging from 0.4 to 0.90, illustrated a decrease in magnitude of the positive c_l–α slope when $M_\infty = 0.6$ when vortex breakdown appeared above the wing and a reversal of the slope in the higher Mach number cases. This difference in trend for the lower and higher Mach number cases was attributed by Erickson to the presence of a strong terminating shock-wave system in the higher Mach number cases. In the current investigation, the vortex lift is found to continue to increase when both symmetric vortex breakdown and no terminating shock-wave system are present above the wing, i.e., $M_\infty = 0.6$, and to decrease when both symmetric vortex breakdown and a terminating shock-wave system are present above the wing, i.e., $M_\infty = 0.8$.

D. Experimental Accuracy

Although the nature of the results presented are qualitative, an effort has been made to establish the numerical accuracy of the observations. The wind-tunnel flow conditions are accurate in Mach number within ± 0.002, in stagnation temperature within 10 K, and in angle of attack within ± 0.2 deg. The geometric accuracy of the various observations made in this investigation is discussed next.

The location of the minimum total pressure location, which is considered to be the definition of the primary vortex core location, is determined via five-hole probe measurements. The accuracy of this determination was evaluated by comparing its location for two different types of model installations and is found to be repeatable within $y/y_{le} = \pm 0.01$ in the spanwise direction and in the vertical direction within $z/y_{le} = \pm 0.02$. A similar analysis of the accuracy of the spanwise surface flow separation location, determined using the oil flow visualization technique, yielded a repeatability of $y = \pm 1$ mm or less than 4% of the local semispan at $x/c_r = 0.5$.

An analytical analysis of the optical system found the inaccuracy in location of phenomena observed in the schlieren images due to the refraction of the light is on the order of 10^{-5} m. The worst-case gradients assumed in this analysis were those encountered by the light ray passing through the center of the vortex core and back along nominally the same path in the SRV images. The transmission images will have a better accuracy than this because the light is only required to make a single pass through the test section to produce those images.

IV. Conclusions

The SRV system is shown to be an effective tool for visualizing the flowfield above the lee side of a delta wing in the transonic flow regime both before and beyond the point of vortex breakdown. The spanwise distribution of the termination shock-wave system, both with and without vortex breakdown present above the wing, is defined via the SRV technique for the first time. The existence of an asymmetric and symmetric vortex breakdown mode is established. The presence of a terminating shock-wave system interacting with the vortex breakdown is shown to have a significant impact on the resulting wing performance.

Acknowledgments

The authors would like to thank E. W. de Keizer and F. J. Donker Duyvis for their technical and creative assistance throughout the course of this project.

References

[1] Muylaert, J. M., "Effect of Compressibility on Vortex Bursting on Slender Delta Wings," von Kármán Inst. for Fluid Dynamics, Project Rept. 1980-21, Rhode St. Genèse, Belgium, July 1980.

[2] Délery, J. M., "Aspects of Vortex Breakdown," *Progress in Aerospace Sciences*, Vol. 30, No. 1, 1994, pp. 1–59.

[3] Donohoe, S. R., and Bannink, W. J., "The Utilization of a High Speed Surface Reflective Visualization System in the Study of Transonic Flow Over a Delta Wing," *Wall Interference, Support Interference and Flow Field Measurements*, AGARD CP-535, Paper 8, 1994.

[4] Donohoe, S. R., Bannink, W. J., and Houtman, E. M., "Surface Reflective Visualization System Study of Vortical Flow Over Delta Wings," *Journal of Aircraft*, Vol. 32, No. 6, 1995, pp. 1359–1366.

[5] Merzkirch, W., *Flow Visualization*, Academic, London, 1987, p. 118.

[6] Miller, D. S., and Wood, R. M., "Leeside Flows Over Delta Wings at Supersonic Speeds," *Journal of Aircraft*, Vol. 21, No. 9, 1984, pp 680–686.

[7] Bannink, W. J., "Some Recent Results on Vortex Bursting on a Delta Wing at High Subsonic Speeds," *Validation of Computational Fluid Dynamics*, AGARD CP-437, Vol. 1, Paper 9, 1988.

[8] Erickson, G. E., Schreiner, J. A., and Rogers, L. W., "On the Structure, Interaction and Breakdown Characteristics of Slender Wing Vortices at Subsonic, Transonic and Supersonic Speeds," AIAA Paper 89-3345, Aug. 1989.

G. Laufer
Associate Editor